Electron Paramagnetic Resonance as a Structural Tool to study Graphene Oxide: Potential-dependence of the EPR response

Bin Wang,[†] Alistair J. Fielding[‡] and Robert A.W. Dryfe[†*]*

[†]School of Chemistry, University of Manchester, Oxford Road, Manchester M13 9PL, United Kingdom

[‡]School of Pharmacy and Biomolecular Science, Liverpool John Moores University, James Parsons Building, Byrom Street, Liverpool, L3 3AF, United Kingdom

AUTHOR INFORMATION

Corresponding Author

[*]Email: a.j.fielding@ljmu.ac.uk (A.J.F.)

[*]Email: robert.dryfe@manchester.ac.uk (R.A.W.D.)

ABSTRACT

Electron paramagnetic resonance (EPR) spectroscopy is reported as a tool to probe the behavior of graphene oxide (GO). The potential-dependent response of GO is reported for the first time, and correlated with the observed electrochemical response. The EPR signal, de-convoluted into two constituent parts, was used along with lineshape simulation and the temperature dependence to probe the electrochemical processes. The EPR signal is found to be well described by two components: the narrower one is associated with unpaired electrons on localised functional groups, and shows a reversible increase as the GO is biased to positive potentials. The Curie behaviour of this component suggests that it increases because of the formation of stable radical species, such as semiquinones, derived from quinones and other carbonyl functional groups found on GO. A stronger dependence of the narrow component with potential, and an elevated g value over 2.0034, is found in alkaline conditions compared to neutral electrolytes, reflecting the greater stability of seminquinone-like species at higher pH. By contrast, the second, broader component of the EPR signal was found to be potential independent. The EPR approach described here offers a solution phase alternative, which can be employed under electrochemical control, to techniques such as X-ray photoelectron spectroscopy and Raman spectroscopy, as a means to probe the structure of GO and related materials.

TOC GRAPHICS

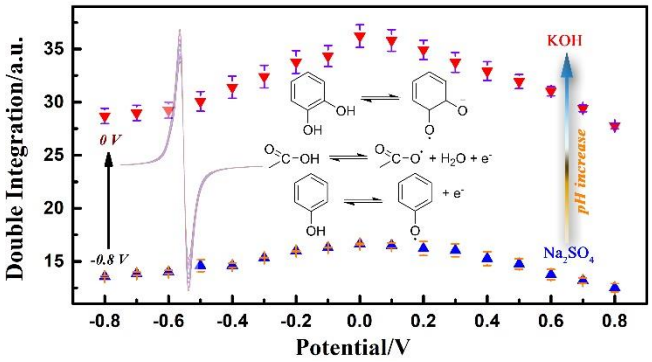

INTRODUCTION

There has been much interest in the application of 2D materials, derived from the prototypical material graphene, in electrochemical energy storage.[1-5] Although microscopic (electron microscopy, atomic force microscopy) and spectroscopic (X-ray photoelectron spectroscopy, Raman spectroscopy) methods are widely used to probe the structure of the materials, and consequently relate the structure to the observed electrochemical response, only the Raman approach is readily compatible with *in situ* solution phase studies. For the use of GO in supercapacitors, for example, it is important to be able to relate structure to function as GO can store charge via classical "double-layer" mechanisms and via pseudo-capacitive routes, involving the oxidation/reduction of oxygen-containing functional groups. The key challenge with supercapacitors is to optimize structure to improve energy density, by improving their capacitance (such as nanostructuring and/or enhancing their pseudo-capacitive component), or maximizing their usable voltage range (by using ionic liquid electrolytes or hybrid supercapacitors).[2,5-9]

Functionalization with oxygen groups is a promising method to enhance supercapacitors because these functional groups provide external pseudo-capacitance and improve the wetting properties of the electrode in aqueous solution.[5, 8, 10-23] For example, functionalized graphene prepared by a low-temperature thermal treatment has a gravimetric capacitance of up to 450 F g^{-1}.[8] In addition, the pseudo-capacitance, imparted to graphene by representative oxygen-containing groups, has been shown to be pH dependent[13, 16, 20]:

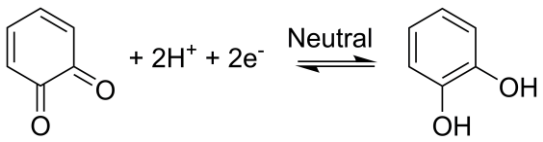

(1)

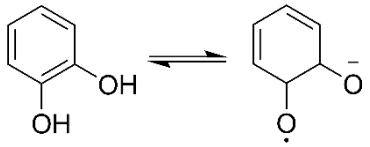

(2)

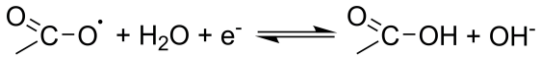

(3)

Quinone groups are generally supposed to cause pseudo-capacitive enhancement in acidic conditions, whereas carboxyl groups are thought to produce the faradaic reactions under alkaline condition, due to the relative ease of oxidation of the carboxylate group at high pH [Eqns. 1-3].[11, 16, 21, 23] Understanding of the charge storage mechanism of oxygen-functionalized graphene at the microscopic level is still lacking, despite the computational approaches to the problem reported in a number of papers.[24-27]

GO is a particularly complex material, both in terms of chemical structure and its re-assembly to form a laminate type material, a form which has been widely used as an electrode for studies of supercapacitance.[28-30] Electron paramagnetic resonance (EPR) spectroscopy has been used previously to study GO, although we are unaware of any previous in situ electrochemical EPR work.[31-42] Recent work by Augustynika-Jablokow *et al*. has shown the existence of slowly relaxing paramagnetic centers in GO attributed to isolated unfunctionalized carbons in highly functionalized regions.[31, 32] Our previous paper described the magnetic properties of GO, without metal impurities associated with its formation, and its pH dependent behavior. This work identified two types of spin on GO: localized sigma "dangling bond" spins associated with defects with a narrow linewidth. By "defect" we mean any functional group or atom that can act as a local "trap" for unpaired electrons. A broader signal is associated with delocalised π electrons from the remaining aromatic domains.[33] The EPR signal of GO was found to be pH-dependent, i.e. the

greatest EPR signal was detected when exposed to aqueous KOH solutions, which was explained in terms of a further oxidative fragmentation of the carbonaceous framework.

In this contribution, *in situ* electrochemical EPR spectroscopy is used to study the potential-dependent response of GO in Na_2SO_4 and KOH (1 M) aqueous electrolytes based on a three electrode capillary cell after a stabilization process due to radical quenching in aqueous solutions (Figure S1). Additionally, temperature-dependent EPR spectroscopy was used to study the relationship between the unpaired spins and structure. We are only aware of one previous study of the potential-dependent EPR response of graphene-based materials, which focusses on graphene (as opposed to GO) prepared by chemical vapor deposition and used a polymer gel electrolyte to reveal a correlation between the spin susceptibility of the material and in-plane conductivity.[43] No specific analysis of the electrochemical response was made in this work on CVD graphene. Additionally, the nature of the spins generated by redox reactions in the alkaline electrolyte employ herein can be tested through the changes in the g value of the EPR spectroscopic signal. Quantitative analysis in different electrolytes shows a correlation between the increased capacitance seen in the alkaline electrolyte, and the spectroscopic signal which we ascribe to the enhanced pseudo-capacitive behavior of the oxygenated functional groups. Further simulations allowed the distribution of the mobile electrons as a function of potential to be investigated, which is also beneficial for understanding the pseudo-capacitive process on graphene-based materials.

Methods

Graphene oxide: GO was prepared by a modified Hummer's method, as reported elsewhere.[44] To remove impurities, such as residual manganese ions and oxidative debris, a simple base wash was used, following previous reports.[33, 42, 45] The base reflux also reduces oxygen functionalities (mainly hydroxyls) by the dehydration reaction, and further acidification was used to re-protonate

the COO^- groups.[42] In particular, GO (1.2 mg/mL) was refluxed in aqueous 0.1 M NaOH (Sigma-Aldrich) for 1 h at 100 °C, and then the treated GO was separated by filtration. The obtained product was dispersed in 0.1 M HCl (Fisher Chemical) followed by reflux for 1 h at 100 °C. The final product was washed by filtration. The flake size of the GO is in the range of 1-5 μm^2:[33] the above washing procedure is followed to eliminate small molecule organic and Mn residues initially present in the sample, which otherwise greatly affect the observed EPR response.[33, 42]

Working electrode: The GO film was prepared by a simple filtration process, described below, and used as the working electrode in the three electrode, *in situ* experiments. The GO suspension (re-dispersed in water by sonication for 2 h at 37 kHz and 350 W effective power, Fisherbrand FB11205 Ultrasonic Cleaner) was filtered onto a PTFE membrane (25 mm diameter hydrophilic PTFE membrane filter with a 0.1 μm pore size and maximum thickness of 140 μm, Merck Millipore Company). After drying at 80 °C, the polymer-supported GO film was twined with Pt wire (99.99% purity, Advent Research Materials Ltd., UK) to bind the film and to function as the current collector for the GO working electrode (WE), in line with our previous report.[46] The surface area of the resultant WE is around 5 mm^2.

The resistance (R_s) of the GO based membrane was measured by the four-probe meter (Jandel Engineering, Linslade, UK) with the nanovoltmeter (2182A) and current source (6220, Keithley Instruments, Cleveland, OH, USA). The conductivity (σ) was calculated based on the membrane thickness (l) and the resistance: $\sigma=1/(l* R_s)$.

The *in situ* electrochemical EPR cell was based on a three-electrode system as previously used (Figure 1),[46] where CE and RE denote the counter and reference electrodes, respectively. All potentials are reported with respect to the RE: the Ag|AgCl RE was prepared by oxidation of partly

exposed Ag wire (99.99% purity, Advent Research Materials Ltd., UK) and Pt mesh (99.99% purity, Advent Research Materials Ltd., UK) was used as the CE. Epoxy was used to seal the connecting joint between the exposed Ag wire contact and the Pt wire used to bind the GO WE. This helps to avoid internal short circuit. The diameter of the quartz capillary is 1 mm.

The potential waveform was applied with a potentiostat ($EmStat^{3+}$ Blue, PalmSens, the Netherlands). The EPR spectra were recorded using a continuous-wave (CW) Bruker EMXmicro spectrometer at room temperature. In all cases, the microwave frequency was approximately 9.8 GHz, and the modulation amplitude was 2 G. Triplicate samples were made for in the *in situ* EPR experiment, with the reported spectra being the average of 20 scans. The spin density of purified GO was found to be $3.5(3) \times 10^{19}$ spins g^{-1} (Figure S2). The quality factor (Q factor) was measured by the Ruby and found to be constant over the potential range used.[46] Temperature dependent experiments (from 4 K to 200 K), to study the origin of the EPR signal as a function of applied potential, were achieved by freezing the electrodes rapidly (within 5 secs) in liquid nitrogen after applying the relevant potential for 5 mins. Temperature calibration was carried out using a temperature sensor (Cernox®, Lake Shore Cryotronics, Inc.) inserted into the sample position. Further details of electron microscopy (used for GO characterization) and EPR signal characterization are provided in the Supporting Information.

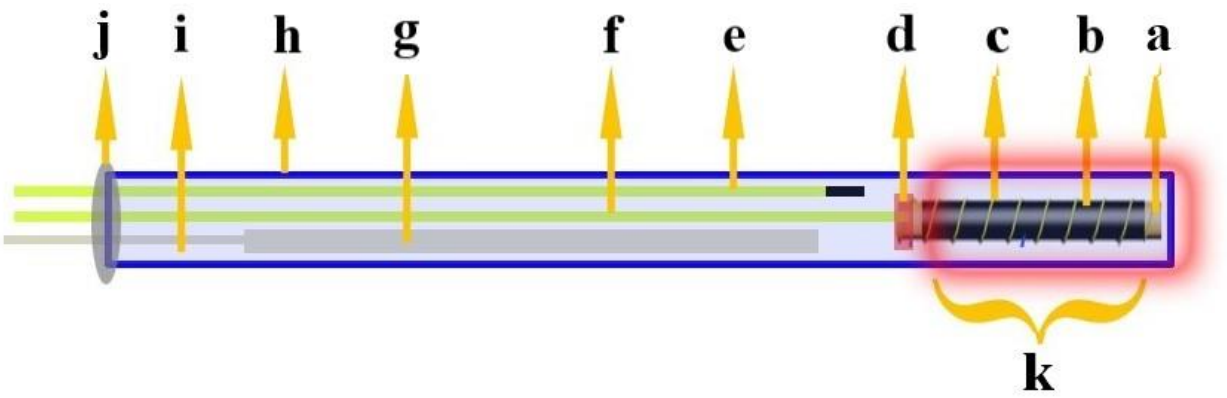

Figure 1. Schematic diagram of the *in situ* EPR cell with a three electrode system in the capillary. a) Supporting Pt wire (diameter 0.5 mm); b) ***WE***, GO membrane coated onto Pt wire, with the length of ~ 2 cm; c) intertwined Pt wire (diameter 0.05 mm); d) Sealant epoxy, prevent the short-circuit, not in the EPR detecting area; e) ***RE***, insulated Ag wire (diameter 0.2 mm, coated with PTFE) with one end oxidized; f) Insulated Ag wire (diameter 0.2 mm, coated with PTFE) to line the ***WE*** and the potentiastant; g) ***CE***, Pt mesh; h) Quartz capillary (diameter 1 mm); i) Aqueous electrolytes, e.g. Na_2SO_4/KOH; j) Sealant epoxy; k) *In situ* cell introduced into the EPR cavity.

Results and Discussion

The oxygen atoms of GO are thought to be distributed amongst various functional groups such as hydroxyl, carbonyl and carboxyl.[33] The electrochemical performance of the GO membrane (thickness of 3 μm, Figure S3) in different pH electrolytes was recorded using the three-electrode configuration: the resultant cyclic voltammograms (CVs) are shown in Figure 2. The voltammetric responses of GO are pH dependent: the capacitance in 1 M KOH (54 F g^{-1} at a scan rate of 50 mV s^{-1}) is higher than that in 1 M Na_2SO_4 solution (44 F g^{-1}). The oxygen-containing functionalities responsible for the faradic reaction are observed more clearly in the CV under alkaline conditions. This increase in capacitance can be attributed to the redox reactions of the carboxyl groups in KOH electrolyte. The capacitance of our GO sample is higher than some reported values for GO (e.g. ~ 27 F g^{-1} in 1 M Na_2SO_4[28]), while it is somewhat lower than other literature, which have generally modified the GO materials (e.g. 135 F g^{-1} in 5.5 M KOH[30]; reduced graphene oxide with a

capacitance to 220 F g^{-1} in 4 M KOH[13]). The lower capacitance in our sample could be related to its low conductivity (3.6 S m^{-1}) and also the limited space within the narrow bore *in situ* EPR cell meaning the GO sample thickness is lower than frequently used in previous reports. Although there have been numerous reported mechanistic explanations of the pH dependence of the capacitance, here we employ in situ EPR spectroscopy to probe GO in different electrolytes.

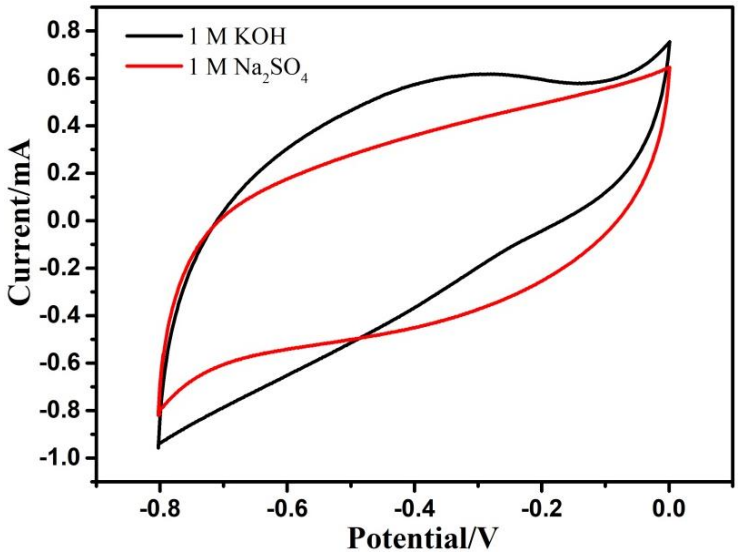

Figure 2. The electrochemical performance of the GO electrode in different electrolytes at a scan rate of 50 mV s^{-1}.

Initially, the GO material was tested at room temperature for slow relaxing spin centers, using in-phase and out-of-phase EPR signals, as described by Augustynika-Jablokow *et al*.[31-32] However, no significant out-of-phase signal was observed (Figure S4) suggesting that faster relaxing centers exist in our material. This apparent discrepancy is very likely caused through differences in preparation and washing procedures. The GO structure is known to be very sensitive to "sample history".[31-37, 42]

The *in situ* electrochemical continuous-wave (CW) 9 GHz EPR study of the GO electrode was carried out by applying a constant potential to the electrode and monitoring the EPR signal. The

cell was cycled 20 times (by cyclic voltammetry at 50 mV s^{-1}, over potential limits from −0.8 V to 0 V in each electrolyte) to obtain a stable response before the in situ EPR experiment. The spectroscopic response obtained from GO during potentiostatic charging and discharging in 1 M Na_2SO_4 is summarized in Figure 3. The EPR signal of the GO electrode was found to increase as the applied potential was swept positive (shown in Figure 3a), and returned to the original when the cell was discharged from 0 V to −0.8 V reversibly, as shown in Figure 3b.

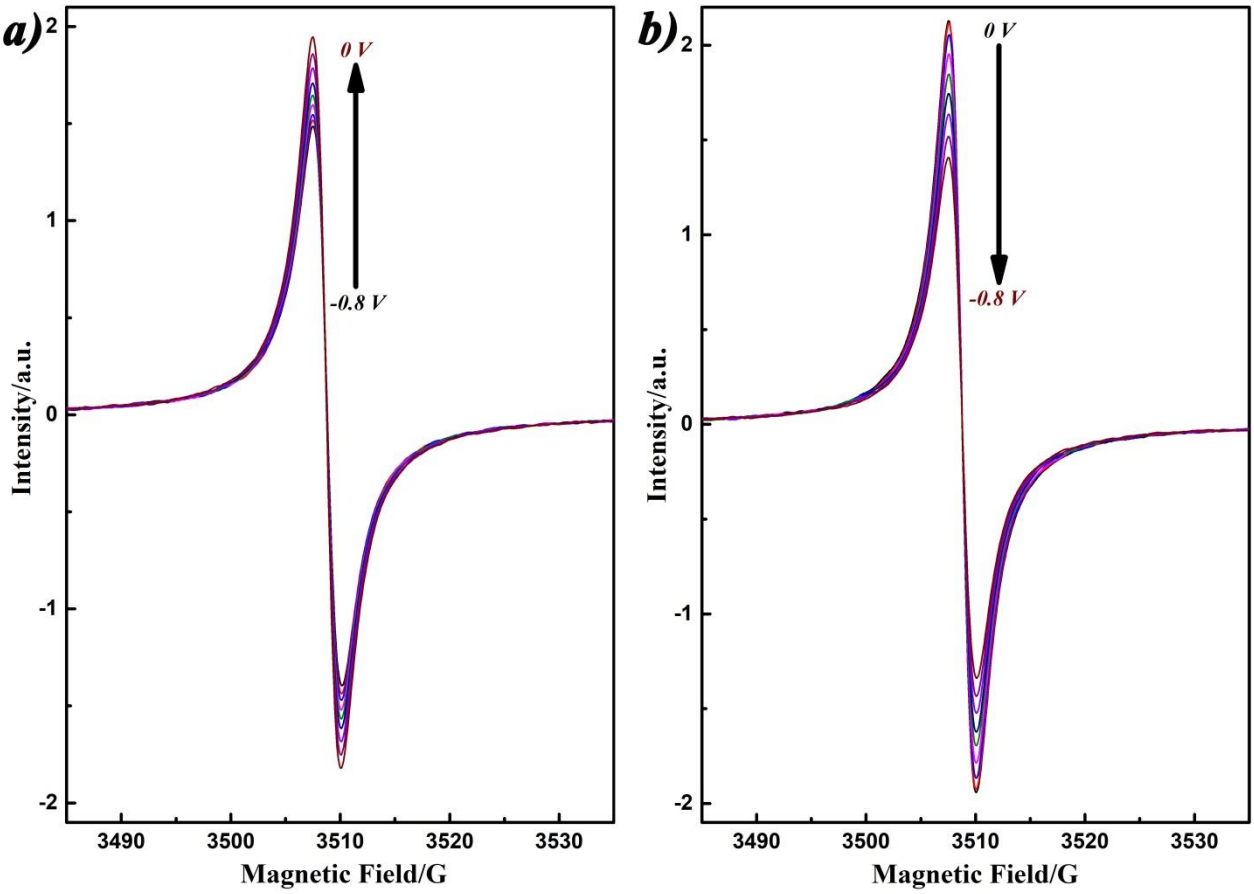

Figure 3. *In situ* EPR response of GO in 1 M Na_2SO_4 over the potential range −0.8 V to 0 V. (a) EPR spectra during charging from −0.8 V to 0 V; (b) EPR spectra during discharging from 0 V to −0.8 V.

The EPR lineshapes are assumed to be described by Lorentzian functions due to the homogeneous distribution of radical species.[47] The EPR spectra in neutral electrolyte can be fitted with two components (Figure 4a, b and Figure S5): a narrow Lorentzian curve with linewidth around 2.5 G; an asymmetric broad Lorentzian curve (asymmetry ratio, A/B ~1.5, Figure S6) with linewidth of 12 G, that is characteristic of conducting samples with mobile electrons. The EPR component with the narrow linewidth indicates a localized state with long spin relaxation times, suggesting defect related spins likely to be oxygen centered radical species from the redox reaction of the oxygenated functional groups.[33, 46] The double integration value (the absolute area value) of the EPR signal, which is related to the spin density of the active material, increases by ~20 % over the positive potential sweep (Figure 4c). Although the narrow resonance shows a reversible increase in spin density, the broad resonance does not change (while the relative ratio changes from 30% to 25% from −0.8 V to 0 V due to the increase of the narrow component). The g value of the narrow curve was found to be 2.0031, suggesting these spins are carbon-based although located on carbon atoms with proximity to oxygen atoms, which is consistent with our interpretation of the electrochemical data. The potential independent broad component has a lower g value of 2.002 and the g value did not show a regular change with potential. The broad curve has been related to conductive π-carriers propagating in the extended aromatic graphite-like structure.[33, 35, 40, 42, 48-50] The linewidth of both components remained constant over the potential range studied.

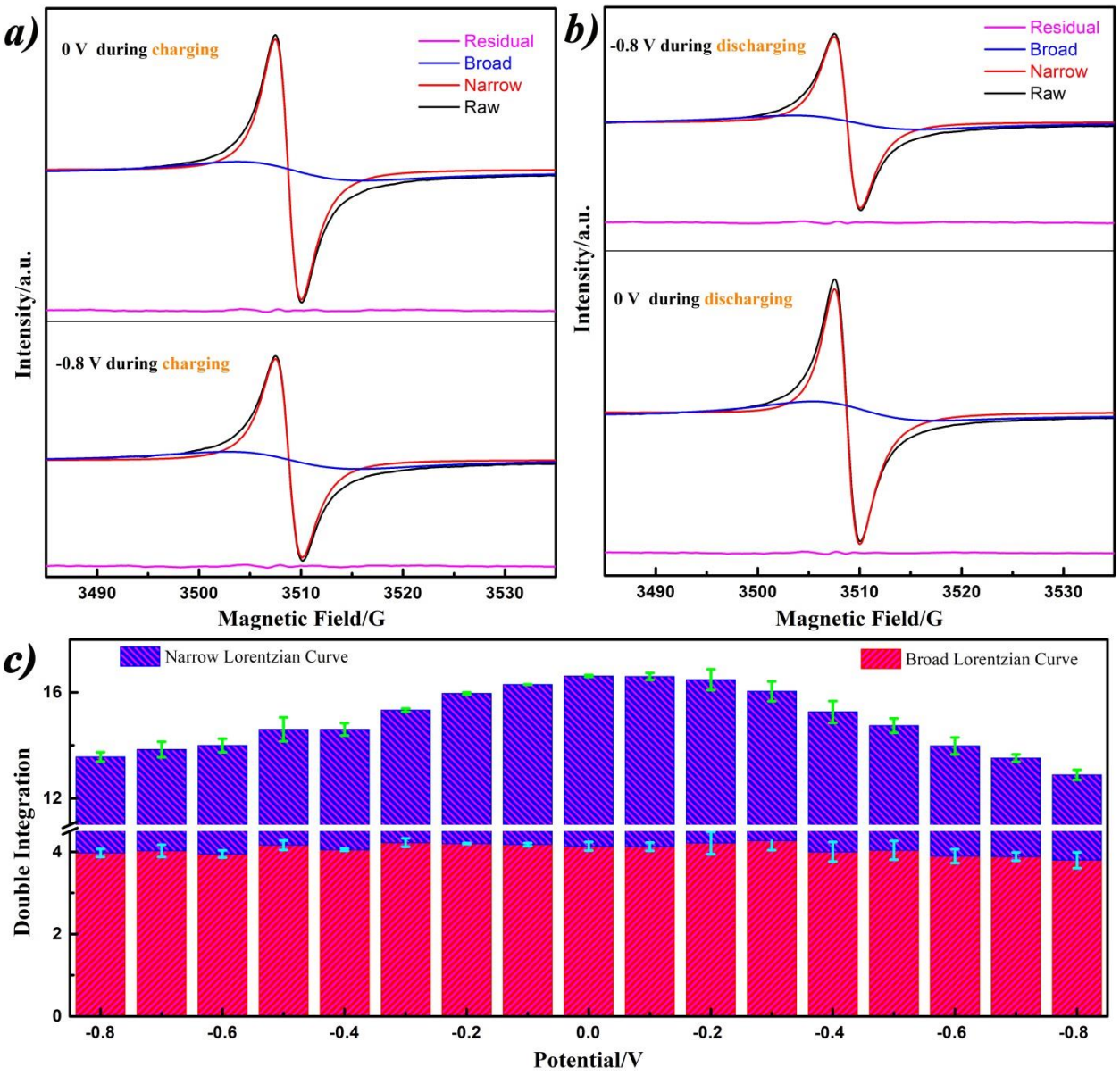

Figure 4. EPR lineshape simulation of GO under potentials in 1 M Na_2SO_4 during (a) charging and (b) discharging; (c) summary of the double integration value of simulated components over charging/discharging

Additionally, an *in situ* EPR experiment of the GO electrode was carried out in a 1 M KOH solution to investigate the enhanced capacitance observed in basic electrolyte (see Figure 2). A similar change to that seen in neutral electrolyte was found, as shown in Figure 5a,b: the EPR

signal of GO in KOH increased with potential and then returned when the potential was decreased from 0 V to −0.8 V.

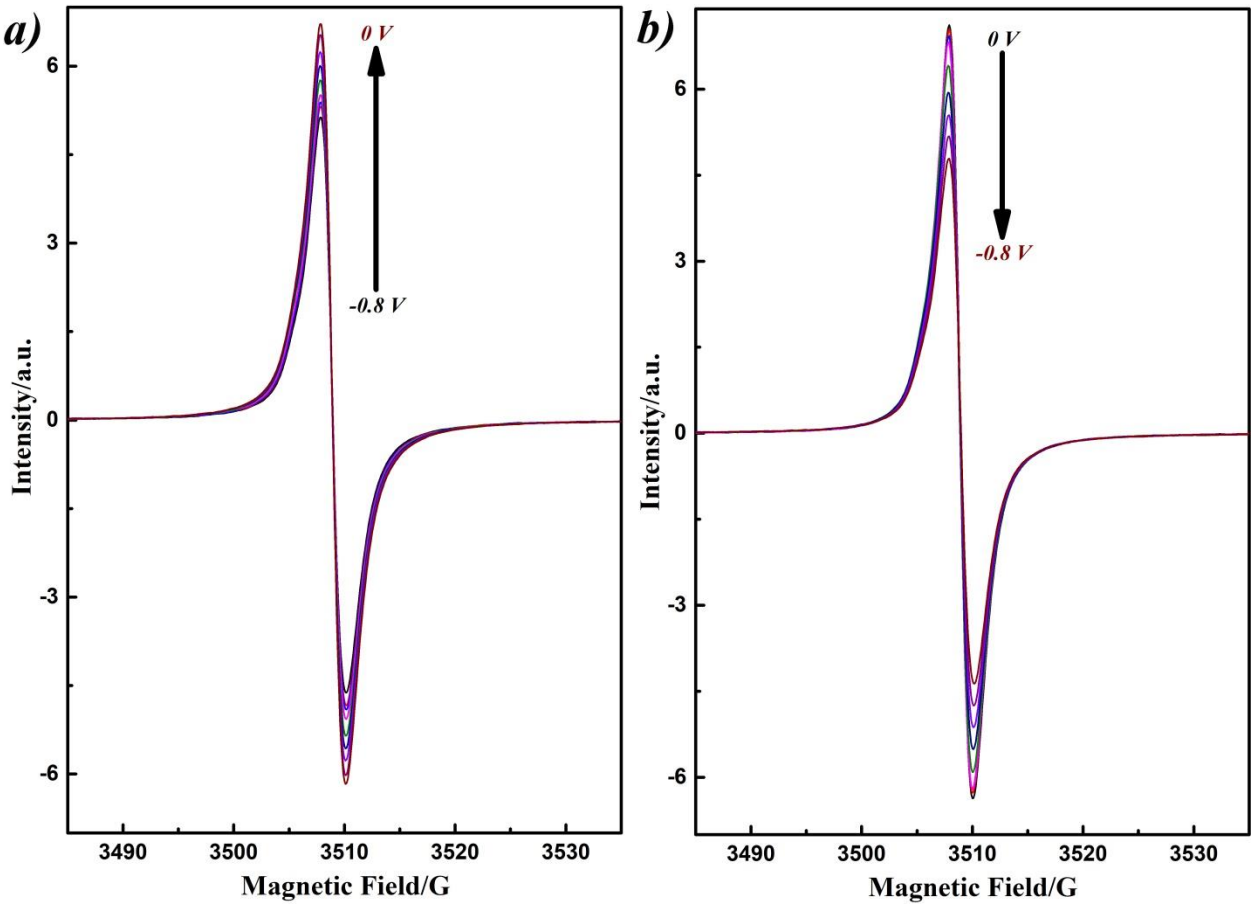

Figure 5. *In situ* EPR experiment of GO in 1 M KOH over the potential range −0.8 V to 0 V. (a) EPR spectra during charging from −0.8 V to 0 V; (b) EPR spectra during discharging from 0 V to −0.8 V.

In this case, however, only a single Lorentzian signal with a linewidth of 2.5 G was required to give an acceptable fit to experiment (see Figure 6a, b): the disappearance of the broad component suggests a more defective structure when the GO was exposed to aqueous KOH.[31] A summary of the spin density change with potential is shown in Figure 6c, with the relative percentage increasing by 27% from −0.8 V to 0 V. The narrow curve has a higher g value, of 2.0034, and presents a stronger potential dependence compared to the neutral electrolyte case (as shown in Figure 7). The

higher g value means more oxygen-centered radical species are generated, which is consistent with the known redox chemistry of common oxygen-containing functional groups (specifically, the favored oxidation of hydroquinone or phenolate groups to semiquinone or phenoxy species, respectively) at high pH.[51] The linewidth was also constant over the potential range.

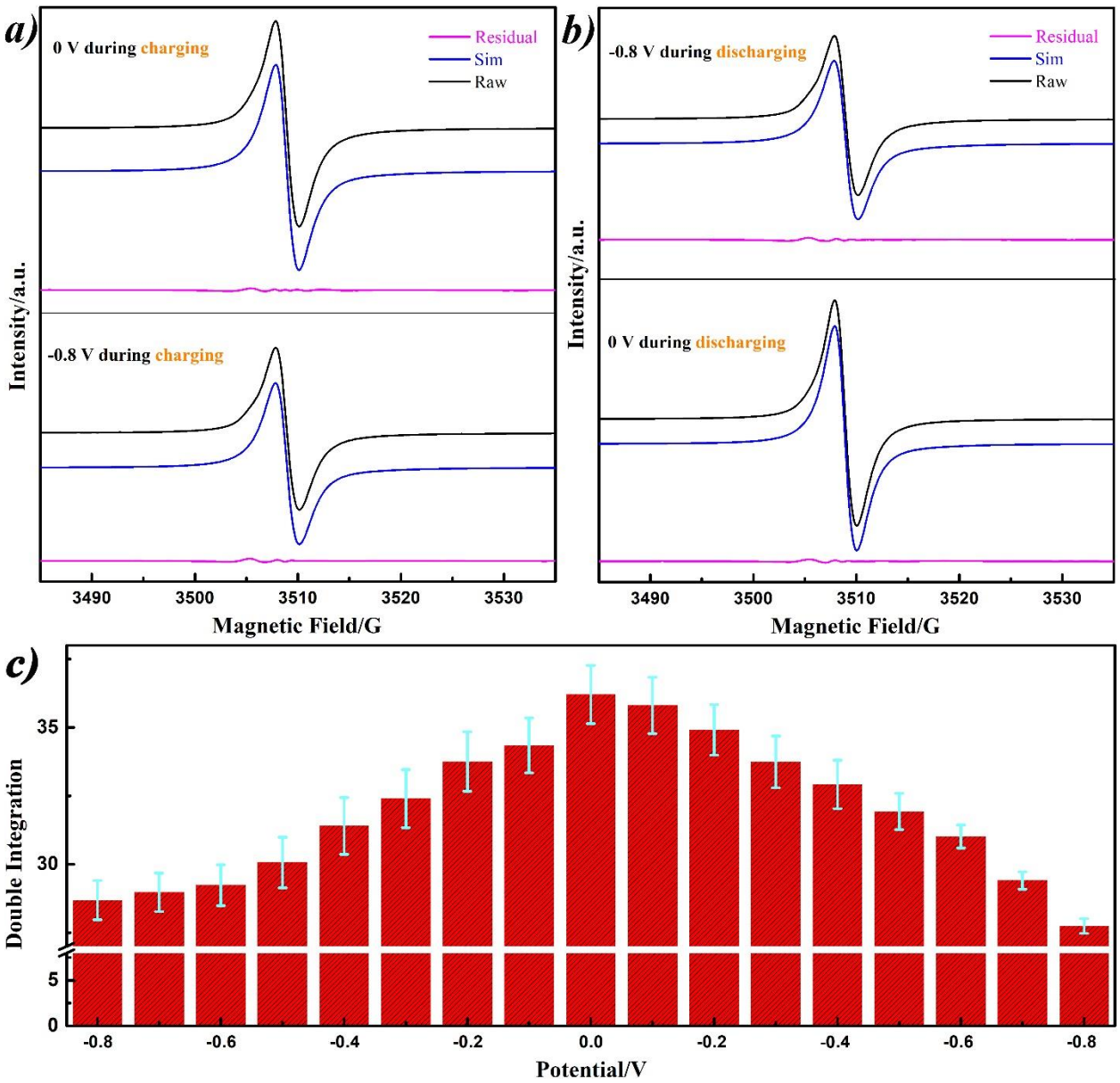

Figure 6. EPR lineshape simulation of GO under potentials in 1 M 1 M KOH during (a) charging and (b) discharging; (c) summary of the double integration value of over charging/discharging.

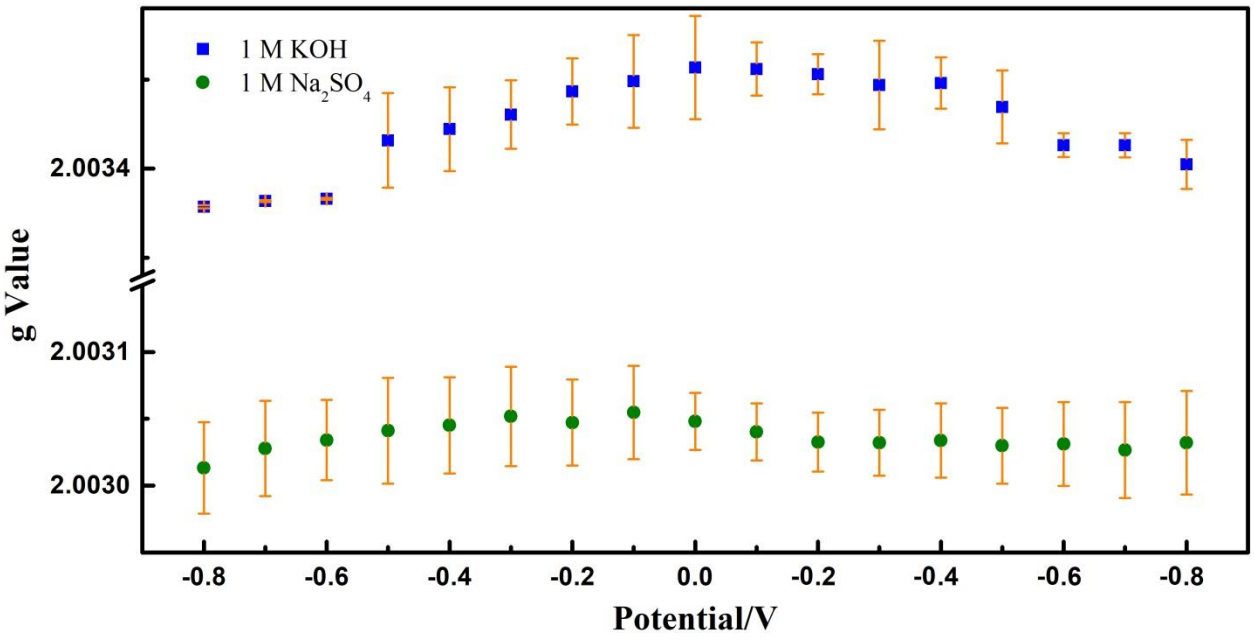

Figure 7. Comparison of the potential dependent g value of the narrow component of the GO electrode in 1 M Na_2SO_4 and KOH electrolytes.

To study the origin of the spins during charging/discharging, the temperature dependence of the EPR signal from GO at 0 V was studied and is shown in Figure 8. The spin susceptibility, calculated from double integration (the absolute value) of the first derivative EPR signal, is fitted by the sum of the Curie-Weiss law and the Pauli law:

$$\chi_{EPR} = \chi_P + \chi_{C-W} = \chi_P + C/(T - T_0) \quad (4)$$

Here χ_{EPR}, χ_P and $\chi_{C\text{-}W}$ stand for the potential-dependent spin susceptibility of the GO electrode, the Pauli susceptibility and the Curie susceptibility, respectively; C is the Curie constant and T_0 is the Curie-Weiss temperature. The Curie-Weiss behavior suggests the narrow signal comes from localized spins including the oxygen-centered radicals formed at defects during the reduction process. The negative Curie-Weiss temperature (T_0, −2.4 K in Na_2SO_4 and −5.4 K in KOH) suggests anti-ferromagnetic behavior, which may be related to the localized states on different sublattices.[52, 53]

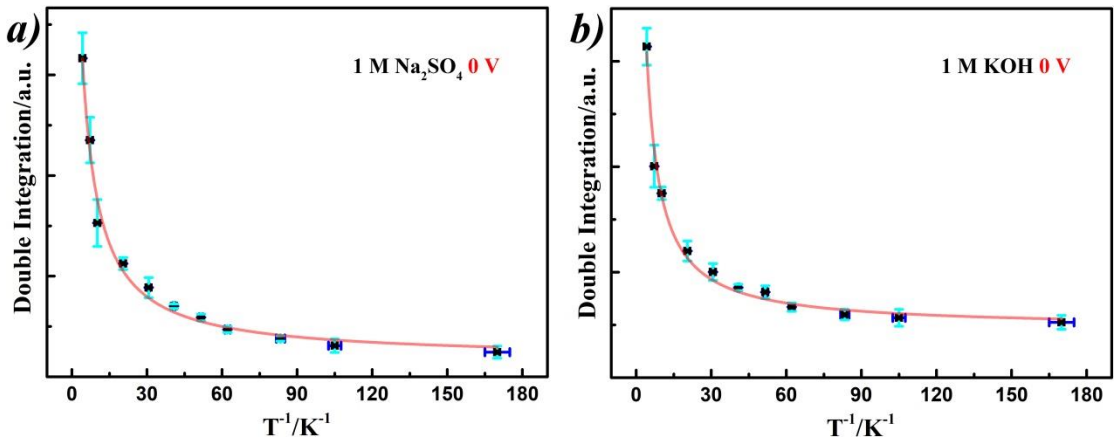

Figure 8. Temperature-dependent EPR behaviour of the GO film at 0 V in different electrolytes: (a) 1 M Na_2SO_4 and (b) 1 M KOH. The temperature was varied from 4.2 K to 200 K. The solid line represents the fitting results of the sum of Curie-Weiss and the Pauli Law (Equation 4).

The *in situ* EPR experiment was carried out to reveal the change of unpaired electron density on GO during its charge and discharge in aqueous solution. GO, according to the Leif-Klinowski model, contains oxygenated functional groups with hydroxyl groups decorating the basal plane, and carboxylate and quinone groups on its edge.[54] The comparison of the CV response of GO (Figure 2) reveals redox peaks in both electrolytes, which have been attributed to the reactions 1-3 (see Introduction, written as reductions):[13] Hydroquinone-type groups are oxidized to quinones in proton-rich conditions (Equation (1)), but can be oxidized to the semiquinone intermediate under alkaline conditions (Equation (2)). The redox reaction of carboxylate groups (Equation (3)) in alkaline electrolyte also contributes to the pseudo-capacitive behavior. Electron transfer between isolated quinone units in the extended structure of the GO is possible because the material possesses some conductivity (*vide supra*) meaning that electrons can be transferred within the solid, at least over limited regions. The same argument can also be applied to the suggested reversible oxidation/reduction of the carboxylate species (Equation 3), assumed to form at high pH. Such a radical would be expected to be highly unstable as part of a small molecule, but would

be stabilized somewhat as part of a more extended pi-system as found in GO.[55] Less distinct redox reactions are found in neutral electrolyte than in KOH electrolyte, leading to lower capacitance, in agreement with previous reports, presumably because the above reactions are less favored – or are less reversible – at lower pH.[13, 20]

The complexity of the structure causes the different origin of the spins: localized spins related to functional groups after oxidation (e.g. semiquinone radicals); the delocalized mobile electrons on the aromatic graphitic-like domains. The broad component of GO in Na_2SO_4 electrolyte was found to be potential independent and the narrow signal shows the major variation in both electrolytes during the *in situ* EPR measurement. Oxidation of the surface-bound oxygen functional groups on the GO as the potential of the latter is swept positive causes the increase of the density of localized spins, reflected in the increased narrow EPR signal with increasing potential seen in Figures 3 and 5.[46] The EPR signal intensity decreases when the potential is swept to negative values, reflecting the resultant depletion of unpaired electron density. The potential dependent narrow component in neutral electrolyte therefore suggests a pseudo-capacitive origin from functionalities such as quinone and carboxylate groups. The variation of the double integration value of the narrow resonance in 1 M KOH (ca. 7, Figure 6c) is much higher than in the neutral electrolyte (ca. 3, Figure 4c), and the g value in 1 M KOH is greater (Figure 7). The higher potential-sensitivity of the narrow resonance in 1 M KOH (Figure 6c) should reflect the greater propensity to form semiquinone radicals (Equation 2). The *in situ* EPR results directly correlate with the enhanced pseudocapacitive process seen in alkaline electrolyte, thus explaining the enhanced capacitance of oxygen-rich carbon materials in alkaline conditions.

To conclude*, in situ* electrochemical EPR spectroscopy has been used to study the capacitive behavior of GO to explore the electron transfer process. The simulation of the spectral lineshape of GO as a function of potential determined that two types of spins exist, each associated with different structures. The narrow signal, which increases during the charging process and reversibly returns when discharged, is related to the generation of more stable semiquinone radicals from the oxidation of hydroquinone at higher pH. The broad component, arising from mobile electrons in extended sp^2 graphitic-like structure, shows potential independent behavior in both electrolytes. Comparison between a neutral electrolyte (Na_2SO_4) and an alkaline electrolyte (KOH) indicated that the increased capacitance in the KOH environment contributes to the pseudo-capacitive behavior of the oxygen functional groups.

ASSOCIATED CONTENT

Supporting Information.

Experimental section includes the characterization of the GO, *in situ* EPR measurement and the temperature dependent measurement, the EPR Lorentzian/Dysonian lineshape simulation. Result section includes the SEM image of the prepared GO membrane, the micrograph of prepared working electrode, the EPR lineshape simulation results and also the g value change results.

AUTHOR INFORMATION

Notes

The authors declare no competing financial interests.

ACKNOWLEDGMENT

We thank the U.K. National EPSRC EPR Service and Facility for support, the EPSRC for funding (grant references: EP/K016954/1, EP/I023879/1 and EP/N032888/1) and the ISCF Faraday Challenge Fast Start project on "Degradation of Battery Materials" made available through grant EP/S003053/1. B.W. is grateful for the award of a President's Doctoral Scholarship from the University of Manchester. We also acknowledge great technical assistance from Mr. Adam Brookfield for the EPR measurements.

REFERENCES

1. Winter, M.; Brodd, R. J. What Are Batteries, Fuel Cells, and Supercapacitors? *Chem. Rev.* **2004,** *104* (10), 4245-4270.

2. Simon, P.; Gogotsi, Y. Materials for Electrochemical Capacitors. *Nat. Mater.* **2008,** *7*, 845.

3. Conway, B. E. *Electrochemical Supercapacitors: Scientific Fundamentals and Technological Applications*. Plenum Publisher: New York, 1999.

4. Conway, B. E. Transition from "Supercapacitor" to "Battery" Behavior in Electrochemical Energy Storage. *J. Electrochem. Soc.* **1991,** *138* (6), 1539-1548.

5. Wang, Y.; Song, Y.; Xia, Y. Electrochemical Capacitors: Mechanism, Materials, Systems, Characterization and Applications. *Chem. Soc. Rev.* **2016,** *45* (21), 5925-5950.

6. Zhang, Q.; Uchaker, E.; Candelaria, S. L.; Cao, G. Nanomaterials for Energy Conversion and Storage. *Chem. Soc. Rev.* **2013,** *42* (7), 3127-3171.

7. Lang, X.; Hirata, A.; Fujita, T.; Chen, M., Nanoporous Metal/Oxide Hybrid Electrodes for Electrochemical Supercapacitors. *Nature Nanotech.* **2011,** *6*, 232.

8. Yan, J.; Wang, Q.; Wei, T.; Jiang, L.; Zhang, M.; Jing, X.; Fan, Z., Template-Assisted Low Temperature Synthesis of Functionalized Graphene for Ultrahigh Volumetric Performance Supercapacitors. *ACS Nano* **2014,** *8* (5), 4720-4729.

9. Fang, Y.; Luo, B.; Jia, Y.; Li, X.; Wang, B.; Song, Q.; Kang, F.; Zhi, L., Renewing Functionalized Graphene as Electrodes for High-Performance Supercapacitors. *Adv. Mater.* **2012,** *24* (47), 6348-6355.

10. Frackowiak, E.; Béguin, F., Carbon Materials for the Electrochemical Storage of Energy in Capacitors. *Carbon* **2001,** *39* (6), 937-950.

11. Bleda-Martínez, M. J.; Maciá-Agulló, J. A.; Lozano-Castelló, D.; Morallón, E.; Cazorla-Amorós, D.; Linares-Solano, A., Role of Surface Chemistry on Electric Double Layer Capacitance of Carbon Materials. *Carbon* **2005,** *43* (13), 2677-2684.

12. Lin, Z.; Liu, Y.; Yao, Y.; Hildreth, O. J.; Li, Z.; Moon, K.; Wong, C. P., Superior Capacitance of Functionalized Graphene. *J. Phys. Chem. C* **2011,** *115* (14), 7120-7125.

13. Oh, Y. J.; Yoo, J. J.; Kim, Y. I.; Yoon, J. K.; Yoon, H. N.; Kim, J. H.; Park, S. B., Oxygen Functional Groups and Electrochemical Capacitive Behavior of Incompletely Reduced Graphene Oxides as a Thin-film Electrode of Supercapacitor. *Electrochim. Acta* **2014,** *116*, 118-128.

14. Hsieh, C. T.; Teng, H., Influence of Oxygen Treatment on Electric Double-Layer Capacitance of Activated Carbon Fabrics. *Carbon* **2002,** *40* (5), 667-674.

15. Okajima, K.; Ohta, K.; Sudoh, M., Capacitance Behavior of Activated Carbon Fibers with Oxygen-Plasma Treatment. *Electrochim. Acta* **2005,** *50* (11), 2227-2231.

16. Chen, C. M.; Zhang, Q.; Zhao, X. C.; Zhang, B.; Kong, Q. Q.; Yang, M. G.; Yang, Q. H.; Wang, M. Z.; Yang, Y. G.; Schlögl, R.; et al., Hierarchically Aminated Graphene Honeycombs for Electrochemical Capacitive Energy Storage. *J. Mater. Chem.* **2012,** *22* (28), 14076-14084.

17. Oda, H.; Yamashita, A.; Minoura, S.; Okamoto, M.; Morimoto, T., Modification of the Oxygen-Containing Functional Group on Activated Carbon Fiber in Electrodes of an Electric Double-Layer Capacitor. *J. Power Sources* **2006,** *158* (2), 1510-1516.

18. Barisci, J. N.; Wallace, G. G.; Baughman, R. H., Electrochemical Studies of Single-Wall Carbon Nanotubes in Aqueous Solutions. *J. Electroanal. Chem.* **2000,** *488* (2), 92-98.

19. Cheng, P. Z.; Teng, H., Electrochemical Responses from Surface Oxides Present on HNO_3-treated Carbons. *Carbon* **2003,** *41* (11), 2057-2063.

20. Andreas, H. A.; Conway, B. E., Examination of the Double-Layer Capacitance of an High Specific-Area C-Cloth Electrode as Titrated from Acidic to Alkaline pHs. *Electrochim. Acta* **2006,** *51* (28), 6510-6520.

21. Centeno, T. A.; Stoeckli, F., The Role of Textural Characteristics and Oxygen-Containing Surface Groups in the Supercapacitor Performances of Activated Carbons. *Electrochim. Acta* **2006,** *52* (2), 560-566.

22. Centeno, T. A.; Stoeckli, F., On the Specific Double-Layer Capacitance of Activated Carbons, in Relation to Their Structural and Chemical Properties. *J. Power Sources* **2006,** *154* (1), 314-320.

23. Kim, H.; Fortunato, M. E.; Xu, H.; Bang, J. H.; Suslick, K. S., Carbon Microspheres as Supercapacitors. *J. Phys. Chem. C* **2011,** *115* (42), 20481-20486.

24. Kerisit, S.; Schwenzer, B.; Vijayakumar, M., Effects of Oxygen-Containing Functional Groups on Supercapacitor Performance. *J. Phys. Chem. Lett.* **2014,** *5* (13), 2330-2334.

25. Park, S.W.; DeYoung, A. D.; Dhumal, N. R.; Shim, Y.; Kim, H. J.; Jung, Y., Computer Simulation Study of Graphene Oxide Supercapacitors: Charge Screening Mechanism. *J. Phys. Chem. Lett.* **2016,** *7* (7), 1180-1186.

26. DeYoung, A. D.; Park, S.W.; Dhumal, N. R.; Shim, Y.; Jung, Y.; Kim, H. J., Graphene Oxide Supercapacitors: A Computer Simulation Study. *J. Phys. Chem. C* **2014,** *118* (32), 18472-18480.

27. Xu, K.; Ji, X.; Chen, C.; Wan, H.; Miao, L.; Jiang, J., Electrochemical Double Layer Near Polar Reduced Graphene Oxide Electrode: Insights from Molecular Dynamic Study. *Electrochim. Acta* **2015,** *166*, 142-149.

28. Liu, Y.; Yan, D.; Li, Y.; Wu, Z.; Zhuo, R.; Li, S.; Feng, J.; Wang, J.; Yan, P.; Geng, Z., Manganese Dioxide Nanosheet Arrays Grown on Graphene Oxide as an Advanced Electrode Material for Supercapacitors. *Electrochim. Acta* **2014,** *117*, 528-533.

29. Jeong, H. K.; Jin, M.; Ra, E. J.; Sheem, K. Y.; Han, G. H.; Arepalli, S.; Lee, Y. H., Enhanced Electric Double Layer Capacitance of Graphite Oxide Intercalated by Poly(sodium 4-styrensulfonate) with High Cycle Stability. *ACS Nano* **2010,** *4* (2), 1162-1166.

30. Stoller, M. D.; Park, S.; Zhu, Y.; An, J.; Ruoff, R. S., Graphene-Based Ultracapacitors. *Nano Lett.* **2008,** *8* (10), 3498-3502.

31. Augustyniak-Jablokow, M. A.; Tadyszak, K.; Strzelczyk, R.; Fedaruk, R.; Carmieli, R., Slow Spin Relaxation of Paramagnetic Centers in Graphene Oxide. *Carbon* **2019**, *152*, 98-105.

32. Augustyniak-Jablokow, M. A.; Fedaruk, R.; Strzelczyk, R.; Majchrzycki, L., Identification of a slow relaxing Paramagnetci Center in Graphene Oxide. *Appl. Magn. Reson.* **2019**, *50*, 761-768.

33. Wang, B.; Fielding, A. J.; Dryfe, R. A. W., Electron Paramagnetic Resonance Investigation of the Structure of Graphene Oxide: pH-Dependence of the Spectroscopic Response. *ACS Appl. Nano Mater.* **2019**, *2*, 19-27.

34. Szabó, T.; Berkesi, O.; Forgó, P.; Josepovits, K.; Sanakis, Y.; Petridis, D.; Dékány, I. Evolution of Surface Functional Groups in a Series of Progressively Oxidized Graphite Oxides. *Chem. Mater.* 2006, *18*, 2740– 2749

35. Diamantopoulou, A.; Glenis, S.; Zolnierkiwicz, G.; Guskos, N.; Likodimos, V., Magnetism in Pristine and Chemically Reduced Graphene Oxide. *J. App. Phys.* **2017,** *121* (4), 043906.

36. Feng, R.; Zhou, W.; Guan, G.; Li, C.; Zhang, D.; Xiao, Y.; Zheng, L.; Zhu, W. Surface Decoration of Graphene by Grafting Polymerization using Graphene Oxide as the Initiator. *J. Mater. Chem.* 2012, *22*, 3982– 3989.

37. Hou, X. L.; Li, J. L.; Drew, S. C.; Tang, B.; Sun, L.; Wang, X. G. Tuning Radical Species in Graphene Oxide in Aqueous Solution by Photoirradiation. *J. Phys. Chem. C* 2013, *117*, 6788– 6793.

38. Ćirić, L.; Sienkiewicz, A.; Gaál, R.; Jaćimović, J.; Vâju, C.; Magrez, A.; Forró, L. Defects and Localization in Chemically-derived Graphene. *Phys. Rev. B: Condens. Matter Mater. Phys.* 2012, *86*, 195139.

39. Komeily Nia, Z. K.; Chen, J. Y.; Tang, B.; Yuan, B.; Wang, X. G.; Li, J. L. Optimizing the Free Radical Content of Graphene Oxide by Controlling its Reduction. *Carbon* 2017, *116*, 703– 712.

40. Rao, S. S.; Stesmans, A.; Wang, Y.; Chen, Y. Direct ESP Evidence for Magnetic Behavior of Graphite Oxide.*Phys. E* 2012, *44*, 1036– 1039.

41. Ćirić, L.; Sienkiewicz, A.; Djokić, D. M.; Smajda, R.; Magrez, A.; Kaspar, T.; Nesper, R.; Forró, L. Size Dependence of the Magnetic Response of Graphite Oxide and Graphene Flakes – an Electron Spin Resonance Study. *Phys. Status Solidi B* 2010, *247*, 2958– 2961.

42. Su, C.; Acik, M.; Takai, K.; Lu, J.; Hao, S. J..; Zheng, Y.; Wu, P.; Bao, Q.; Enoki, T.; Chabal, Y. J.; Ping Loh, K., Probing the catalytic activity of porous graphene oxide and the origin of this behaviour. *Nat. Commun.* **2012**, *3*, 1298.

43. Fujita, N.; Matsumoto, D.; Sakurai, Y.; Kawahara, K.; Ago, H.; Takenobu, T.; Marumoto, K., Direct Observation of Electrically Induced Pauli Paramagnetism in Single-Layer Graphene using ESR Spectroscopy. *Sci. Rep.* **2016,** *6*, 34966.

44. Hummers, W. S.; Offeman, R. E., Preparation of Graphitic Oxide. *J. Am. Chem. Soc.* **1958**, *80*(6), 1339-1339.

45. Rourke, J. P.; Pandey, P. A.; Moore, J. J.; Bates, M.; Kinloch, I. A.; Young, R. J.; Wilson, N. R., The Real Graphene Oxide Revealed: Stripping the Oxidative Debris from the Graphene-like Sheets. *Angew. Chem. Int. Ed.* **2011**, *50*(14), 3173-3177.

46. Wang, B.; Fielding, A. J.; Dryfe, R. A. W., In situ electrochemical electron paramagnetic resonance spectroscopy as a tool to probe electrical double layer capacitance. *Chem. Commun.* **2018**, *54*(31), 3827-3830.

47. Chechik, V.; Carter, E.; Murphy, D. Electron Paramagnetic Resonance; Oxford University Primers, U.K., 2016.

48. Tampieri, F.; Silvestrini, S.; Riccò, R.; Maggini, M.; Barbon, A., A Comparative Electron Paramagnetic Resonance Study of Expanded Graphites and Graphene. *J. Mater. Chem. C* **2014,** *2* (38), 8105-8112.

49. Enoki, T.; Takai, K., The Edge State of Nanographene and the Magnetism of the Edge-State Spins. *Solid State Commun.* **2009,** *149* (27), 1144-1150.

50. Joly, V. L. J.; Takahara, K.; Takai, K.; Sugihara, K.; Enoki, T.; Koshino, M.; Tanaka, H. Effect of Electron Localization on the Edge State Spins in a Disordered Network of Nanographene Sheets. *Phys. Rev. B* **2010**, *81*, 115408.

51. Guin, P. S.; Das, S.; Mandal P. S., Electrochemical Reduction of Quinones in Different Media: A Review. *Int. J. Electrochem.* **2011**, 816202.

52. Augustyniak-Jabłokow Maria, A.; Tadyszak, K.; Maćkowiak, M.; Yablokov Yurii, V., EPR Evidence of Antiferromagnetic Ordering in Single-Layer Graphene. *Phys. Status Solidi RRL* **2011,** *5* (8), 271-273.

53. Augustyniak-Jabłokow, M. A.; Tadyszak, K.; Maćkowiak, M.; Lijewski, S., ESR Study of Spin Relaxation in Graphene. *Chem. Phys. Lett.* **2013,** *557*, 118-122.

54. He, H.; Riedl, T.; Lerf, A.; Klinowski, J., Solid-State NMR Studies of the Structure of Graphite Oxide. *J. Phys. Chem.* **1996,** *100* (51), 19954-19958.

55. Stathi, P.; Gournis, D.; Deligiannakis, Y.; Rudolf, P., Stabilization of Phenolic Radicals on Graphene Oxide: an XPA and EPR Study. *Langmuir* **2015**, *31* (38), 10508-10516.